Chaos
An Interdisciplinary Journal of Nonlinear Science

Identifying causality drivers and deriving governing equations of nonlinear complex systems

Cite as: Chaos **32**, 103128 (2022); https://doi.org/10.1063/5.0102250
Submitted: 08 June 2022 • Accepted: 01 October 2022 • Published Online: 31 October 2022

Haochun Ma, Alexander Haluszczynski, Davide Prosperino, et al.

Identifying causality drivers and deriving governing equations of nonlinear complex systems

Cite as: Chaos **32**, 103128 (2022); doi: 10.1063/5.0102250
Submitted: 8 June 2022 · Accepted: 1 October 2022 ·
Published Online: 31 October 2022

Haochun Ma,[1,2] Alexander Haluszczynski,[2] Davide Prosperino,[2] and Christoph Räth[3,a)]

AFFILIATIONS

[1]Ludwig-Maximilians-Universität München, Department of Physics, Schellingstraße 4, 80799 Munich, Germany
[2]Allianz Global Investors, risklab, Seidlstraße 24, 80335 Munich, Germany
[3]Deutsches Zentrum für Luft- und Raumfahrt (DLR), Institut für KI Sicherheit, Wilhelm-Runge-Straße 10, 89081 Ulm, Germany

[a)]**Author to whom correspondence should be addressed:** christoph.raeth@dlr.de

ABSTRACT

Identifying and describing the dynamics of complex systems is a central challenge in various areas of science, such as physics, finance, or climatology. While machine learning algorithms are increasingly overtaking traditional approaches, their inner workings and, thus, the drivers of causality remain elusive. In this paper, we analyze the causal structure of chaotic systems using Fourier transform surrogates and three different inference techniques: While we confirm that Granger causality is exclusively able to detect linear causality, transfer entropy and convergent cross-mapping indicate that causality is determined to a significant extent by nonlinear properties. For the Lorenz and Halvorsen systems, we find that their contribution is independent of the strength of the nonlinear coupling. Furthermore, we show that a simple rationale and calibration algorithm are sufficient to extract the governing equations directly from the causal structure of the data. Finally, we illustrate the applicability of the framework to real-world dynamical systems using financial data before and after the COVID-19 outbreak. It turns out that the pandemic triggered a fundamental rupture in the world economy, which is reflected in the causal structure and the resulting equations.

Understanding cause–effect relationships is a key challenge in many areas of science, as it forms the basis for developing analytical and predictive models. However, while methods for causal inference are constantly evolving, finding the drivers of causality is a critical aspect that is often not adequately addressed. Particularly when analyzing complex nonlinear systems, it is very useful to know whether causality stems from linear or nonlinear properties. In this work, we separate the causality in linear and nonlinear contributions and observe that a significant part can be attributed to nonlinear properties. Furthermore, we present a framework by which knowledge of the causal structure can be directly translated into equations that describe the underlying data. Potentially, this methodology can be used to find equations for real systems that allow for precise analysis and prediction.

I. INTRODUCTION

Causality, as one of the basic principles of scientific thought, has been intensively researched over many generations and different disciplines. Throughout history, interpretations of causality have evolved with the increasing effort and complexity of physical theories. While in Newton's classical understanding action and reaction were defined as simultaneously coupled, Einstein introduced a temporal and spatial component by defining causality as events connected by the cone of light.[1] Subsequently, the disruption of quantum mechanics led to a probability-dominated understanding of physics, where causality is an unimaginable concept in a non-deterministic world. With the advent of chaos theory, causality was placed in the context of stability and equilibria of dynamical systems, which became known to the general public as the butterfly effect.[2]

Encouraged by the explosion of computation resources, the development of causal inference methods took a similar but accelerated path. Beginning with Granger causality in the 1960s,[3] many techniques of increasing complexity were developed, ranging from information-theoretic measures[4] to state-space reconstruction methods;[5] Runge[6] provides an excellent overview.

However, while causal inference is primarily concerned with measuring the presence of causality, research on its properties and drivers has remained secondary. A first step in this direction was taken by Paluš *et al.*[7] who developed a diagnostic test for identifying nonlinear dynamic relationships in time series based on mutual information. Another approach, using Fourier transform surrogates, was taken by Haluszczynski *et al.*,[8] who separated linear and nonlinear contributions of mutual information to capture nonlinear correlations in financial data. The contribution of nonlinearity to connectivity in climate data was quantified by Hlinka *et al.*[9]

While initial approaches for deriving governing equations from data in the 1990s were based on applying the flow method by inter alia Breeden and Hübler[10] and Eisenhammer *et al.*,[11] research on this topic has expanded considerably in the last few decades. In the context of nonlinear dynamical systems, Brunton *et al.*[12] introduced sparse identification on the chaotic Lorenz attractor. Other techniques include automated inference of dynamics[13] and machine learning approaches.[14]

In this work, we combine the inference and analysis of causality with the derivation of governing equations in nonlinear complex systems. Therefore, we separate the linear and nonlinear contributions to causality using Fourier transform surrogates and develop a transparent rationale based only on the causalities to derive the differential equations.

II. BENCHMARK MODELS

In this work, we first validate our approach on four synthetic systems before demonstrating its applicability on a real-world example. If not stated otherwise, we solve the differential equations of the synthetic system using the Runge–Kutta method[15] for $T = 10\,000$ steps and a discretization of $dt = 0.01$. We discard the initial transient of $T = 50\,000$ steps for the analyses.

A. Lorenz system

In order to analyze the effect of nonlinearity on the causality structure, we introduce two additional parameters λ_1 and λ_2 to control the nonlinear terms of the Lorenz system, which models atmospheric convection,[16]

$$\begin{aligned} \frac{dx}{dt} &= \sigma(y - x), \\ \frac{dy}{dt} &= x(\rho - \lambda_1 z) - y, \\ \frac{dz}{dt} &= \lambda_2 xy - \beta z, \end{aligned} \tag{1}$$

where the standard parametrization is $\sigma = 10$, $\rho = 28$, $\beta = 8/3$, and $\lambda_1 = \lambda_2 = 1$. The implied linear and nonlinear connections between the variables are depicted in Fig. 1.

Figure 2 illustrates the attractor for a selection of different parameter configurations: While the system diverges for nonlinearity degrees less or equal to 0, the upper bounds can be chosen arbitrarily as we do not observe significant changes to the butterfly form even for extreme values ($\lambda_1, \lambda_2 \approx 1000$).

B. Halvorsen system

While the nonlinearity terms of the Lorenz system are mixed products of two different variables, the circulant Halvorsen system[17] entails quadratic nonlinearities,

$$\begin{aligned} \frac{dx}{dt} &= ax - 4y - 4z - \lambda y^2, \\ \frac{dy}{dt} &= ay - 4z - 4x - \lambda z^2, \\ \frac{dz}{dt} &= az - 4x - 4y - \lambda x^2, \end{aligned} \tag{2}$$

where $a = 1.3$ and $\lambda = 1$ are the standard parameters.

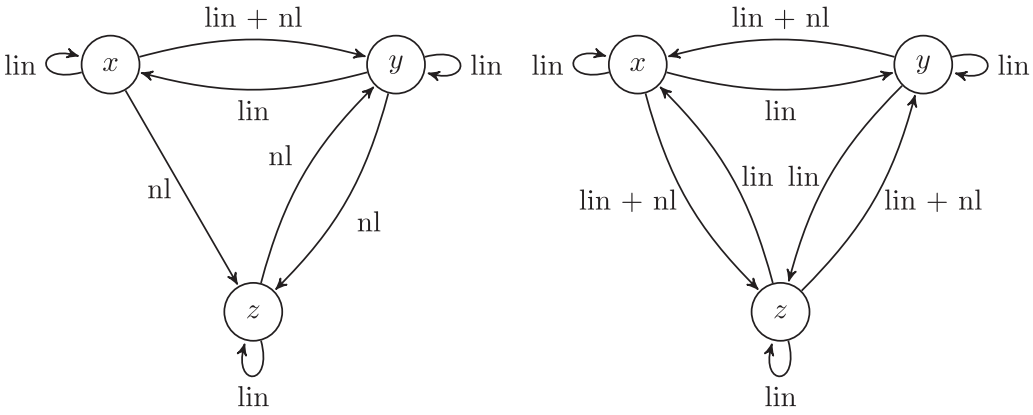

FIG. 1. Causality pictogram of the Lorenz (left) and Halvorsen (right) system. The linear (lin) and nonlinear (nl) causal links are depicted by the labeled arrows.

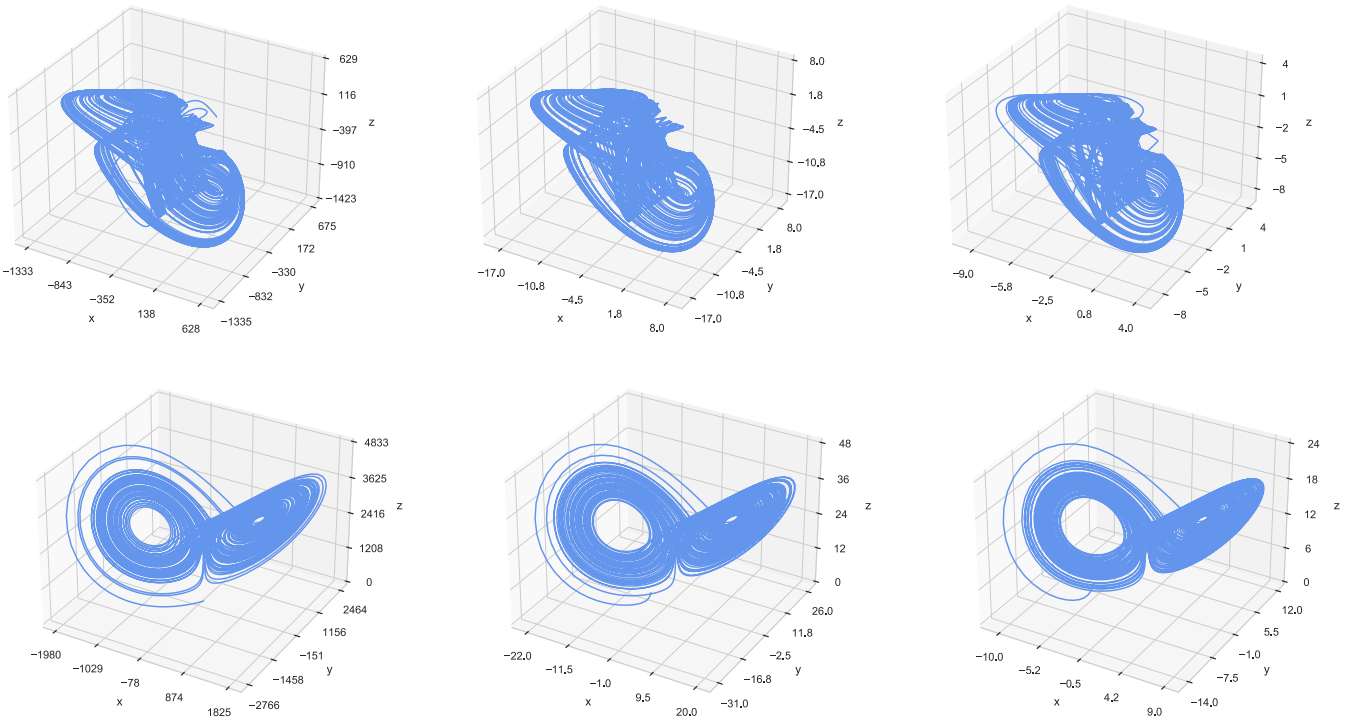

FIG. 2. Lorenz (top row) and Halvorsen (bottom row) attractors for different degrees of nonlinearity. While the standard parameters for the Lorenz system are set at $\sigma = 10$, $\beta = 8/3$, $\rho = 28$, the nonlinearity parameters from left to right are $\lambda_1 = \lambda_2 = 0.01$, $\lambda_1 = \lambda_2 = 1$, and $\lambda_1 = \lambda_2 = 2$. For the Halvorsen system, the nonlinearity parameters from left to right are $\lambda = 0.01, 1, 2$.

Analogously, we control the nonlinearity strength through the additional parameter λ. As observed for the Lorenz system, the basic form of the Halvorsen attractor also stays intact for variations in nonlinearity, as illustrated in Fig. 2.

C. Fully linear system

In order to verify that a fully linear system leads to only linear causality to be detected, we include the following system into our analysis:

$$\begin{aligned} \frac{dx}{dt} &= \sin(y), \\ \frac{dy}{dt} &= x + z, \\ \frac{dz}{dt} &= x - y. \end{aligned} \tag{3}$$

We would like to point out that purely linear systems do not exhibit chaotic behavior and that this system serves solely as a verification of our methods. The time series for the first $T = 30\,000$ steps after the initial transient are shown in Fig. 3.

D. Fully nonlinear system

In contrast, we also include a fully nonlinear system specified by the following equations:[18]

$$\begin{aligned} \frac{dx}{dt} &= \alpha yz, \\ \frac{dy}{dt} &= 1 - z^2, \\ \frac{dz}{dt} &= \beta x^3 + yz, \end{aligned} \tag{4}$$

where we set $\alpha = \beta = 1$ for chaotic behavior. The attractor of this system is depicted in Fig. 3.

E. Stock indices

In order to demonstrate the applicability of our framework to real-world systems, we consider the global financial market around the outbreak of the COVID-19 pandemic. Therefore, we choose the six major economies and their corresponding MSCI stock indices between November 2018 and May 2021: Europe (EU), United States (US), China (CN), Emerging Markets (EE), Japan (JP), and Pacific excluding Japan (PX). We convert the daily prices p_t to log-returns,

$$x_t \equiv \log p_t - \log p_{t-1}, \tag{5}$$

and divide the series into two phases: the time before the outbreak of the pandemic in February 2020 and the time after. This yields two sets of time series each with length $T = 325$, respectively. The

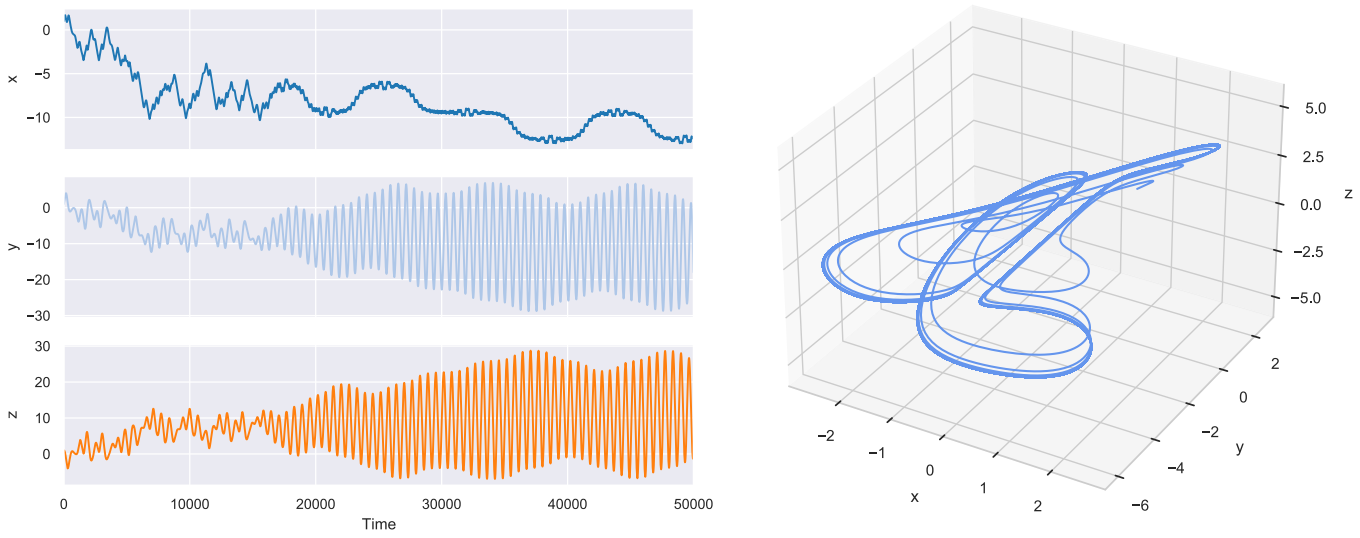

FIG. 3. Time series of the fully linear (left) and nonlinear (right) systems. The left figure depicts the first $T = 30\,000$ time series steps after the initial transient of the fully linear system, while the right figure shows the attractor of the fully nonlinear system.

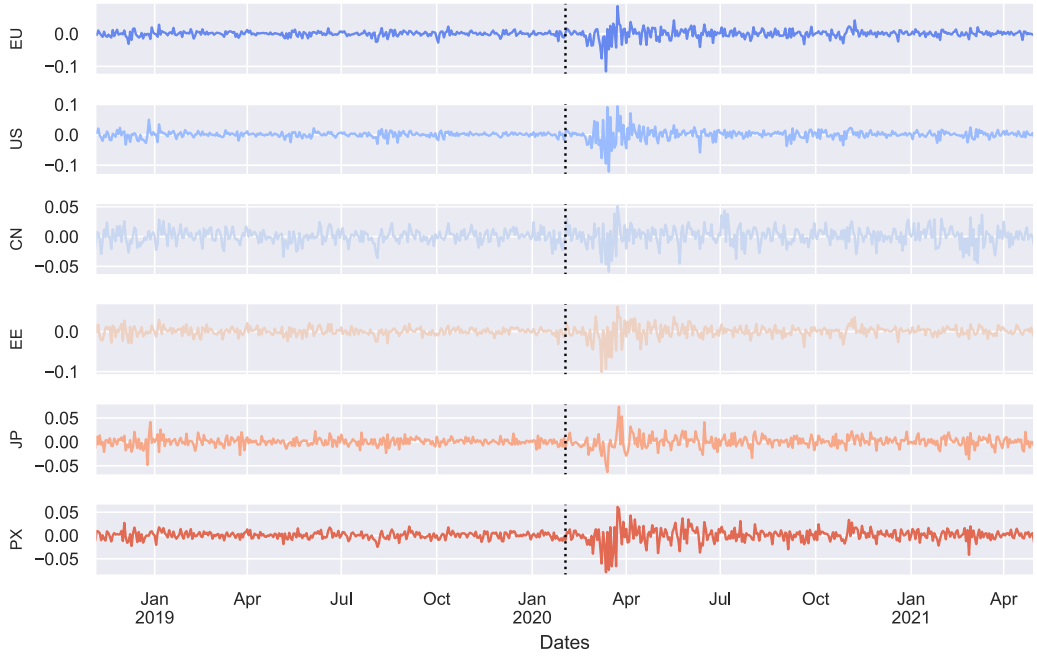

FIG. 4. Log returns of stock indices from six major economies. The illustrated time series are Europe (EU), United States (US), China (CN), Emerging Markets (EE), Japan (JP), and Pacific excluding Japan (PX). The black dashed vertical line depicts the outbreak of the COVID-19 pandemic in February 2020.

structural change in the dynamics of the stock indices triggered by the outbreak of COVID-19 can be observed in Fig. 4.

III. METHODS

In the following, we present the methods used in this work, which we assign to four different categories: Causality measures, Fourier transform surrogates, network measures, and the derivation of governing equations.

A. Causality measures

We select three techniques representing the main categories currently used in causal inference[6]—however, it is important to note that our framework is applicable to any method capable of detecting nonlinear causality.

1. Granger causality using linear autoregressive model

As one of the first causal inference approaches, Granger causality (GC) tests whether the prediction error of the next time step of a time series $\boldsymbol{y}$ can be decreased by including the history of another time series $\boldsymbol{x}$—in this case, $\boldsymbol{x}$ is said to Granger cause $\boldsymbol{y}$.[19] Its original form compares the prediction error of a restricted autoregression model,

$$\hat{y}_t = \sum_{\tau=1}^{\tau_{max}} \alpha_\tau y_{t-\tau} + \varepsilon_t, \tag{6}$$

to its corresponding augmented model,

$$\hat{y}_t = \sum_{\tau=1}^{\tau_{max}} \alpha_\tau y_{t-\tau} + \sum_{\tau=1}^{\tau_{max}} \beta_\tau x_{t-\tau} + \eta_t, \tag{7}$$

where α_τ and β_τ are coefficients at lag τ and ε_t and η_t denote independent error terms. While GC is mostly used as a binary statistical hypothesis test,[19] we quantify the strength of the causal coupling using the following normalization:

$$\psi_{GC}(\boldsymbol{x}, \boldsymbol{y}) = 1 - \min\left\{1, \left(\frac{\mathrm{RSS}_{aug}}{\mathrm{RSS}_{rest}}\right)^2\right\}, \tag{8}$$

where RSS_{rest} and RSS_{aug} denote the residual sum of squares (RSS) of the restricted and augmented model, respectively. Hence, when the regression of the augmented model performs better than the restricted model ($\mathrm{RSS}_{aug} < \mathrm{RSS}_{rest}$), the fraction on the right-hand side is small—this implies stronger causality.

Since there exists no universal method to determine the optimal maximum lag τ_{max}, we repeat the procedure for several values of the maximum lag τ_{max} and average the result. Therefore, we take $N = 20$ equally distributed values between 1 and the time series length T: $\tau_{max} = 1, T/N, 2T/N, \ldots, T$. As we do not find a significant difference, we conclude that the average is a good estimator within the scope of this work.

2. Transfer entropy

Following the proof of equivalence between GC and transfer entropy (TE) for Gaussian variables,[20] the measure introduced by Schreiber[4] has been widely regarded as the information-theoretical extension of GC. Analogously, TE quantifies the reduction of uncertainty on future values of $\boldsymbol{y}$ by accounting for past values of $\boldsymbol{x}$ given the history of $\boldsymbol{y}$. In essence, it is a special case of conditional mutual information (CMI),

$$\begin{aligned}\psi_{TE}(\boldsymbol{x}, \boldsymbol{y}) &\equiv I(\boldsymbol{y}; \boldsymbol{x}_{t-1:} \mid \boldsymbol{y}_{t-1:}) \\ &= H(\boldsymbol{y}, \boldsymbol{y}_{t-1:}) + H(\boldsymbol{x}_{t-1:}, \boldsymbol{y}_{t-1:}) \\ &\quad - H(\boldsymbol{x}_{t-1:}, \boldsymbol{y}, \boldsymbol{y}_{t-1:}) - H(\boldsymbol{y}_{t-1:}),\end{aligned}$$

where the colon indicates all previous steps of the time series and where H denotes the (joint) entropy of the time series calculated via

$$H(\boldsymbol{x}, \boldsymbol{y}) = -\sum_{t=1}^{T}\sum_{t=1}^{T} p(x_t, y_t) \log p(x_t, y_t). \tag{9}$$

For better comparability to other inference methods, we propose the following normalization:

$$\psi_{TE}(\boldsymbol{x}, \boldsymbol{y}) \mapsto \frac{\psi_{TE}(\boldsymbol{x}, \boldsymbol{y})}{\sqrt{H(\boldsymbol{y}, \boldsymbol{y}_{t-1:})\, H(\boldsymbol{x}, \boldsymbol{x}_{t-1:})}}. \tag{10}$$

Our reasoning for this normalization is based on our interpretation of TE as an asymmetric causal measure, similar to covariance, which is rescaled to obtain the normalized cross correlation.

We would like to point out that the calculation of empirical probability densities p and, hence, information-theoretic measures raise unexpected difficulties exceeding the scope of this work. While it is common to use histograms with equally distributed bins to estimate densities, Mynter[21] showed that this method potentially leads to biases since the estimation is highly dependent on the partition details—hence, finding a robust estimator is non-trivial. However, for the purpose of our research, we find that for time series of length T a number of $\sqrt{T/4}$ equally distributed bins performs reasonably well. This was also empirically confirmed by Baur and Räth[22] who used this binning configuration for the construction of generalized local states in reservoir computing. Furthermore, it is worth mentioning that TE might capture false causalities depending on the dimension of conditioning.[23]

3. Convergent cross mapping

Another category of causal inference is state-space methods such as convergent cross-mapping (CCM), which was developed by Sugihara *et al.*[5] Its underlying idea is based on Takens' theorem, which states that the full state-space can be reconstructed from a single embedded coordinate of the system, also called shadow manifold. Due to transitivity, two coordinates within one system can then be mapped to each other through neighboring states in their respective shadow manifolds—this enables a cross prediction. Hence, if $\boldsymbol{x}$ causes $\boldsymbol{y}$, the prediction of the future $\hat{y}_t$ using the shadow manifold $\mathcal{M}_{\boldsymbol{x}}$ should be identical to the actual value y_t. In the context of CCM, the prediction is extended from a single value to a series. Therefore, both time series are divided into training and test sets, where the former are used to construct the shadow manifolds and the latter serve as benchmarks to evaluate the prediction performance.

While CCM is defined as the Pearson correlation ρ between the prediction $\hat{\boldsymbol{y}}|\mathscr{M}_x$ and the test set of $\boldsymbol{y}$, we propose another evaluation measure, the correlation distance $d = \sqrt{2\,(1-\rho)}$, in order to rescale the correlation to a positive interval. This entire procedure is repeated for an increasing training set fraction, which delivers a series $\boldsymbol{d}$ consisting of D correlation distances. This series should theoretically converge to a maximum since the prediction is enhanced for finer resolutions of the shadow manifolds.

While originally CCM requires visual judgment of the convergence, we introduce an algorithmic approach using overlapping sliding windows of size $\boldsymbol{d}$. For each window, we calculate the standard deviation and set a threshold of 0.1. The convergence is fulfilled if the standard deviation decreases continuously and falls below the preset threshold. If $\boldsymbol{d}$ converges, we calculate the mean of its last five values in order to smooth outliers. In case of non-convergence, we set the CCM causality to 0,

$$\psi_{CCM}\left(\boldsymbol{x},\boldsymbol{y}\right) \equiv \begin{cases} \frac{1}{5}\sum_{i=1}^{5} d_{D-5+i} & \text{if } d \text{ converges} \\ 0 & \text{else} \end{cases} \in [0,1]\,. \tag{11}$$

We would like to point out that there exist reservations toward CCM regarding some synthetically created systems—however, its wide range of successful applications is testament to its importance for causal inference.[24] We determined the optimal lag by finding the first minimum of the lagged mutual information—this yielded a lag $\tau = 1$. The optimal embedding dimension $\kappa = 3$ was found by using the false-nearest-neighbor algorithm.[25]

4. Limits of causality measures

We would like to point out that we are aware of the limitations of the causal inference methods presented and of causal inference in general. However, in this paper, we use them only to illustrate a framework of how causality can be partitioned into linear and nonlinear contributions and how, assuming correct measurements, governing equations can be derived. It is beyond the scope of this paper to analyze whether they measure true causality and how robust the methods are. For a more detailed discussion of these points, we refer to their original papers Granger,[3] Schreiber,[4] and Sugihara *et al.*[5]

With respect to GC, we recognize that its main requirement, separability of variables, poses problems, especially when applied to deterministic dynamical systems.[19] Therefore, GC only serves as a verification for our analysis, since it is based on autoregression and should, therefore, only capture causality arising from linear properties. We refer to Ref. 3 for more details.

Furthermore, we are aware that TE and CCM work with reconstructed spaces and that their application to variables within an attractor has theoretical weaknesses. However, the analysis in this paper is performed on simulated data and not on a theoretical basis. We refer the reader to Cummins *et al.*[26] for a detailed discussion of the effectiveness of state-space reconstruction methods in determining causality.

Lastly, we would like to note that we are aware that real-world system can be contaminated by different kinds of noise, which affects the performance of our methods. However, these issues lie beyond the scope of this work since they are addressed in the papers which describe the causality inference methods. Since the methods work when the causality graphs are correct, their robustness to noise lies entirely in the robustness of the individual inference models against noise. We refer to Overbey and Todd[27] and Krishna and Tangirala[28] for analyses on TE and CCM, respectively. Empirically, we find our method to be robust to white noise for Signal-to-Noise ratios (SNRs) > 50 dB.

B. Fourier transform surrogates

In order to dissect the causality structure of time series systems into contributions from linear and nonlinear contribution drivers, we utilize Fourier transform (FT) surrogates. They destroy the nonlinear characteristics of a time series $\boldsymbol{x}$ while keeping the linear ones unaffected.[29]

1. Algorithm

First, we perform a Fourier transformation to separate the linear properties into the amplitudes and the nonlinear ones into the phases. Through randomizing the phases of its Fourier transformation by adding uniformly distributed numbers $\boldsymbol{\phi}_k$, solely the nonlinear features are destroyed. Hence, the back-transformation only contains the linear properties of the time series,

$$\tilde{\boldsymbol{x}}^{(k)} = \mathscr{F}^{-1}\left\{\mathscr{F}\{\boldsymbol{x}\}\, e^{i\boldsymbol{\phi}_k}\right\}. \tag{12}$$

We increase the robustness of our results by averaging measures that are calculated on surrogate time series, over multiple realizations of random phases. Unless otherwise specified, we repeat our measurements for $K = 10$ realizations. A discussion on surrogate generation is provided by Räth *et al.*[30]

2. Surrogate-based measures

Within the scope of this work we understand a bivariate measure $\psi\left(\boldsymbol{x},\boldsymbol{y}\right)$ as a function that maps two time series to a real number. Hence, we define its corresponding surrogate measure as the average over K surrogate realizations of both time series,

$$\psi^{surro}\left(\boldsymbol{x},\boldsymbol{y}\right) \equiv \frac{1}{K}\sum_{k=1}^{K}\psi\left(\tilde{\boldsymbol{x}}^{(k)},\tilde{\boldsymbol{y}}^{(k)}\right). \tag{13}$$

As indicated by the superscript k, we add the same random phases to both time series within one realization. This leaves the phase differences unaffected, which, for example, preserves the Pearson correlation.[31]

Furthermore, we define the cross-measure by only surrogating the first time series in the argument,

$$\psi^{cross}\left(\boldsymbol{x},\boldsymbol{y}\right) \equiv \frac{1}{K}\sum_{k=1}^{K}\psi\left(\tilde{\boldsymbol{x}}^{(k)},\boldsymbol{y}\right), \tag{14}$$

and analogously define the reverse as the anti-measure,

$$\psi^{anti}\left(\boldsymbol{x},\boldsymbol{y}\right) \equiv \frac{1}{K}\sum_{k=1}^{K}\psi\left(\boldsymbol{x},\tilde{\boldsymbol{y}}^{(k)}\right). \tag{15}$$

The intuition behind the cross- and anti-measure is to analyze the influence of the linear part of x on y under the measure ψ and vice versa.

3. Nonlinear measures

In the next step, we use these alterations to construct nonlinearity measures extending the idea of nonlinear correlation.[8] Therefore, we assume every measure to be composed of a linear part, represented by the surrogate, and a remaining nonlinear part.

Hence, the most intuitive form is given by the difference,

$$\psi^{nl} \equiv \psi - \psi^{surro}. \tag{16}$$

As we rule out negative nonlinearities attributing them to spurious effects, we propose the measure

$$\psi^{nl} \equiv \max\{0, \psi - \psi^{surro}\}. \tag{17}$$

Further nonlinearity measures can be easily derived by, e.g., normalization or interchanging surro-, cross-, and anti-measures.

C. Evaluation of causality matrices

Given an N-dimensional time series $\mathscr{S} = \{\boldsymbol{x}_1, \ldots, \boldsymbol{x}_N\}$, we can hence compute the causality matrix corresponding to an arbitrary measure $\psi(\boldsymbol{x}, \boldsymbol{y})$,

$$\Psi(\mathscr{S}) \equiv \begin{pmatrix} \psi(\boldsymbol{x}_1, \boldsymbol{x}_1) & \ldots & \psi(\boldsymbol{x}_1, \boldsymbol{x}_N) \\ \psi(\boldsymbol{x}_2, \boldsymbol{x}_1) & \ldots & \psi(\boldsymbol{x}_2, \boldsymbol{x}_N) \\ \vdots & \ddots & \vdots \\ \psi(\boldsymbol{x}_N, \boldsymbol{x}_1) & \ldots & \psi(\boldsymbol{x}_N, \boldsymbol{x}_N) \end{pmatrix},$$

which fully describes the explicit links between the individual variables. In the case of causality measures, they are similar to an adjacency matrix representing finite graphs—hence, the entries $\Psi_{i,j}$ quantify the causal flow from x_i to x_j.

Especially for high-dimensional systems, it is useful to directly evaluate the measure of the whole system. Therefore, we develop intuitive matrix measures, which map a matrix Ψ to a real number. As indicated, a possibility could be to construct a graph from the measure matrix and to compute its corresponding properties. However, as causality measures do not necessarily fulfill the conditions of mathematical distances, we propose the matrix mean

$$\mu_{mean}(\Psi) \equiv \frac{1}{N^2 - N} \sum_{i=1}^{N} \sum_{j=1}^{N} (1 - \delta_{i,j}) \left|\Psi_{i,j}\right|, \tag{18}$$

where we use the Kronecker delta $\delta_{i,j}$ to dismiss the diagonal entries of the matrix since $\psi(\boldsymbol{x}, \boldsymbol{x})$ is equivalent for arbitrary time series $\boldsymbol{x}$.

Considering our focus on causality measures, causality should only be present in a system if no impasse exists which breaks the causal chain. Therefore, we use the geometric mean as it only returns

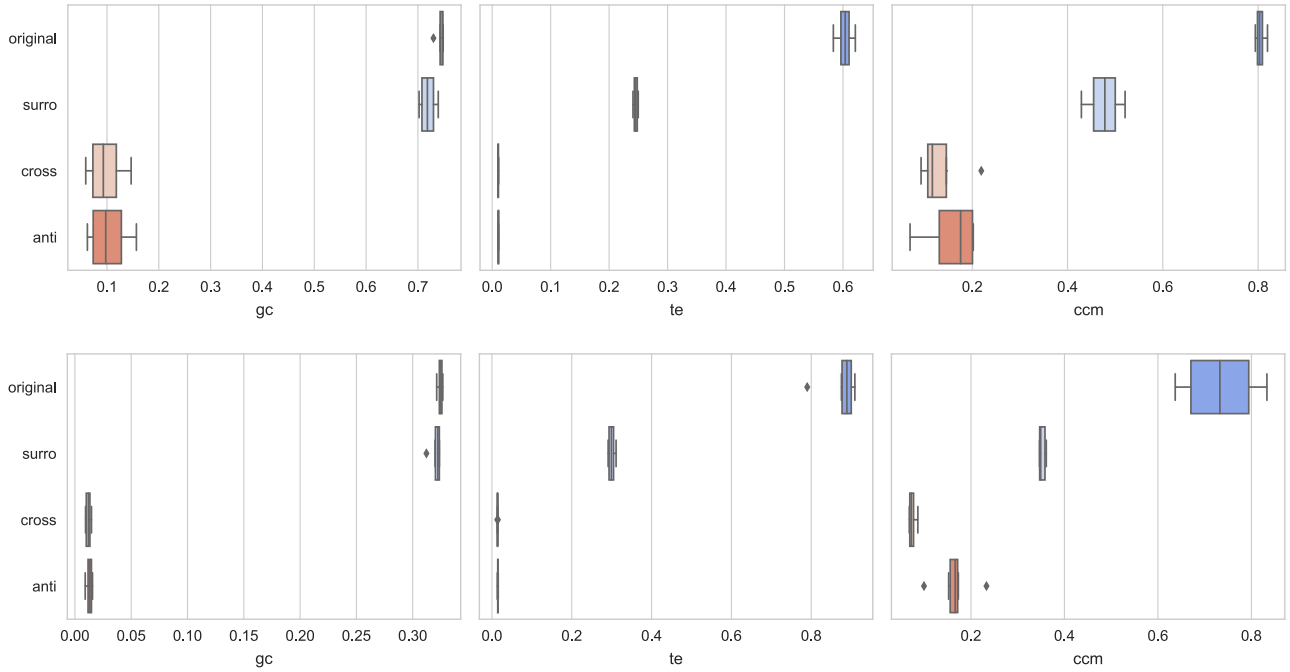

FIG. 5. Causality box plots of the standard Lorenz (top row) and Halvorsen (bottom row) systems. We compute the mean of the original-, surro, cross-, and anti-matrices for GC, TE, and CCM, respectively. The sample consists of 50 simulations under the standard configuration. The surrogate-causalities are averaged over $K = 10$ surrogate realizations. The Lozenge symbols indicate outliers according to the interquantile range (IQR).[32]

a nonzero value if all entries are nonzero,

$$\mu_{geo}(\Psi) \equiv \left(\prod_{i=1}^{N} \prod_{j=1}^{N} (1 - \delta_{i,j}) |\Psi_{i,j}| + \delta_{i,j} \right)^{\frac{1}{N^2 - N}}. \quad (19)$$

Note that we include the matrix diagonals for cross- and anti-measures since their entries offer insights into the linear structure of the individual time series.

D. Derivation of governing equations

While extracting governing equations from data is key to build models in diverse fields of science,[12] existing methods often require sophisticated and specifically tailored algorithms. The major difficulty stems from the problem that there is an infinite number of possible governing equations that represent a finite time series. Even though the number of possibilities reduces for increasing length, the individual terms stay unidentifiable.

Hereby, we illustrate a simple rationale to derive equations directly from the causality matrices inferred from the underlying time series data. Therefore, we assume that the time series stem from a deterministic dynamical system, where a finite sample suffices to identify its underlying causal structure. Hence, by separating linear and nonlinear causalities, the terms of the governing equations become separately deducible. Thus, we argue that the causal structure can be fully described by a linear matrix differential equation and a nonlinear part,

$$\frac{d\boldsymbol{x}}{dt} = \left(\frac{d\boldsymbol{x}}{dt}\right)_{lin} + \left(\frac{d\boldsymbol{x}}{dt}\right)_{nl} = \Psi^{lin}\boldsymbol{x} + \Psi^{nl} \odot \boldsymbol{x}^n,$$

where $\odot$ denotes our rationale for deriving the nonlinear terms and the superscript n indicates an n-dimensional Cartesian product. For simplicity, we assume all nonlinearity terms to be of order $n = 2$. However, this can be easily extended which is primarily relevant for high-dimensional systems.

First, we extract the linear terms from the surrogate- and cross-matrices. While the cross-matrix represents the linear causal flow of a variable to itself, we can extract the flow of the other variables from the surrogate-matrix,

$$\Psi^{lin} = \delta_{i,j}\Psi^{cross}_{i,j} + (1 - \delta_{i,j})\Psi^{surro}_{i,j}. \quad (20)$$

Since we discard entries smaller than a preset threshold $\theta = 0.1$ attributing them to inaccuracies of the causal inference, the individual equations are given by

$$\left(\frac{dx_j}{dt}\right)_{lin} = \sum_{i}^{N} \Theta\left(\Psi^{lin}_{i,j} - \theta\right) x_i, \quad (21)$$

where Θ is the Heaviside-function.

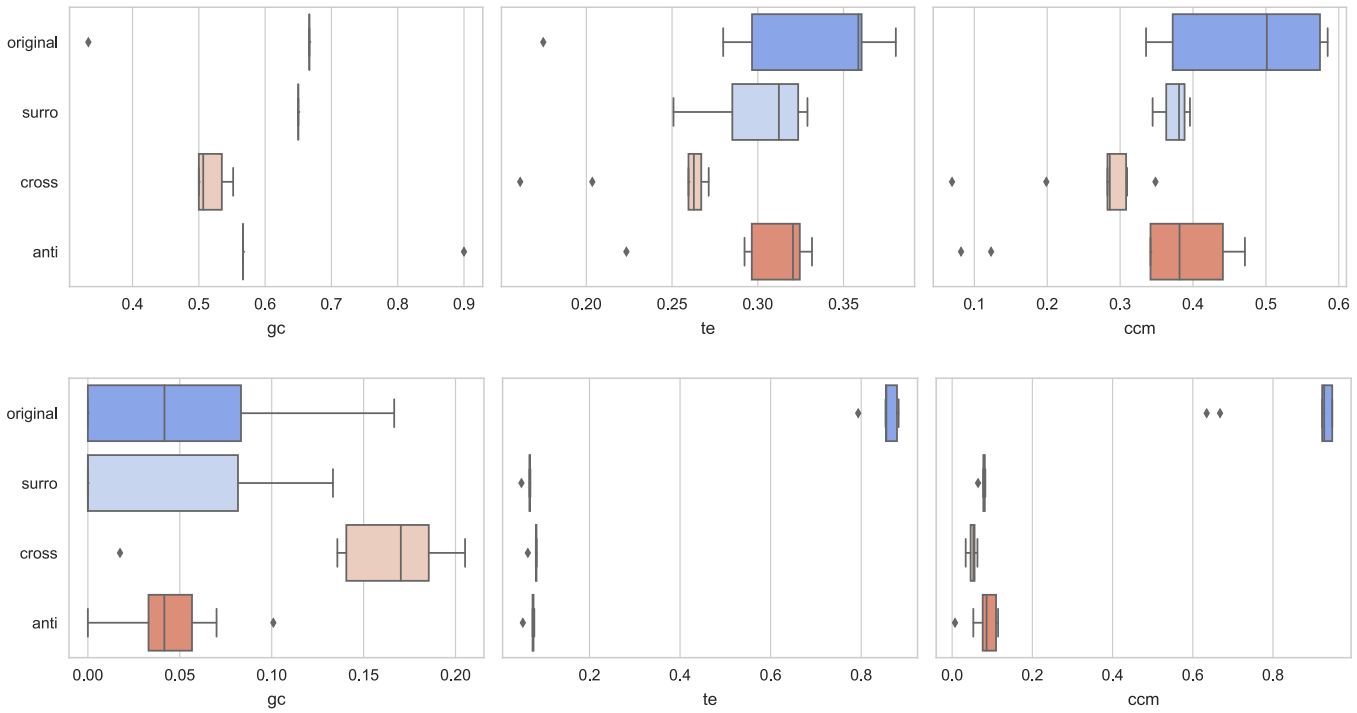

FIG. 6. Causality box plots of the fully linear (top row) and nonlinear (bottom row) systems. We compute the mean of the original-, surro, cross-, and anti-matrices for GC, TE, and CCM, respectively. The sample consists of 50 simulations under the standard configuration. The surrogate-causalities are averaged over $K = 10$ surrogate realizations. The Lozenge symbols indicate outliers according to the interquantile range.

In the next step, we calculate the nonlinear causality-matrix Ψ^{nl} using the original- and surrogate-matrices. Since it incorporates inaccuracies stemming from two causal inferences, we raise the threshold to 2θ. The nonlinear part of the equations can then be constructed by adhering to two simple rules,

- If in one column x_j of Ψ^{nl} only one entry $x_i \neq x_j$ exceeds the threshold, then the nonlinear term entering the equation is

$$\left(\frac{dx_j}{dt}\right)_{nl} = \Theta\left(\Psi^{nl}_{i,j} - 2\theta\right) x_i^2, \tag{22}$$

since we reason that the entire nonlinear causal flow of the system must be accumulated in x_i.

- If multiple entries $\{x_k, x_{k+1}, \ldots, x_l\}$ in Ψ^{nl} exceed the threshold, then all permutation of pairs enter the equation

$$\left(\frac{dx_j}{dt}\right)_{nl} = \sum_{i=k}^{n} \sum_{j\leq i}^{l} \Theta\left(\Psi^{nl}_{i,j} + \Psi^{nl}_{j,i} - 4\theta\right) x_i x_j,$$

since we argue that the nonlinear causal flow must be split between all possible pairs.

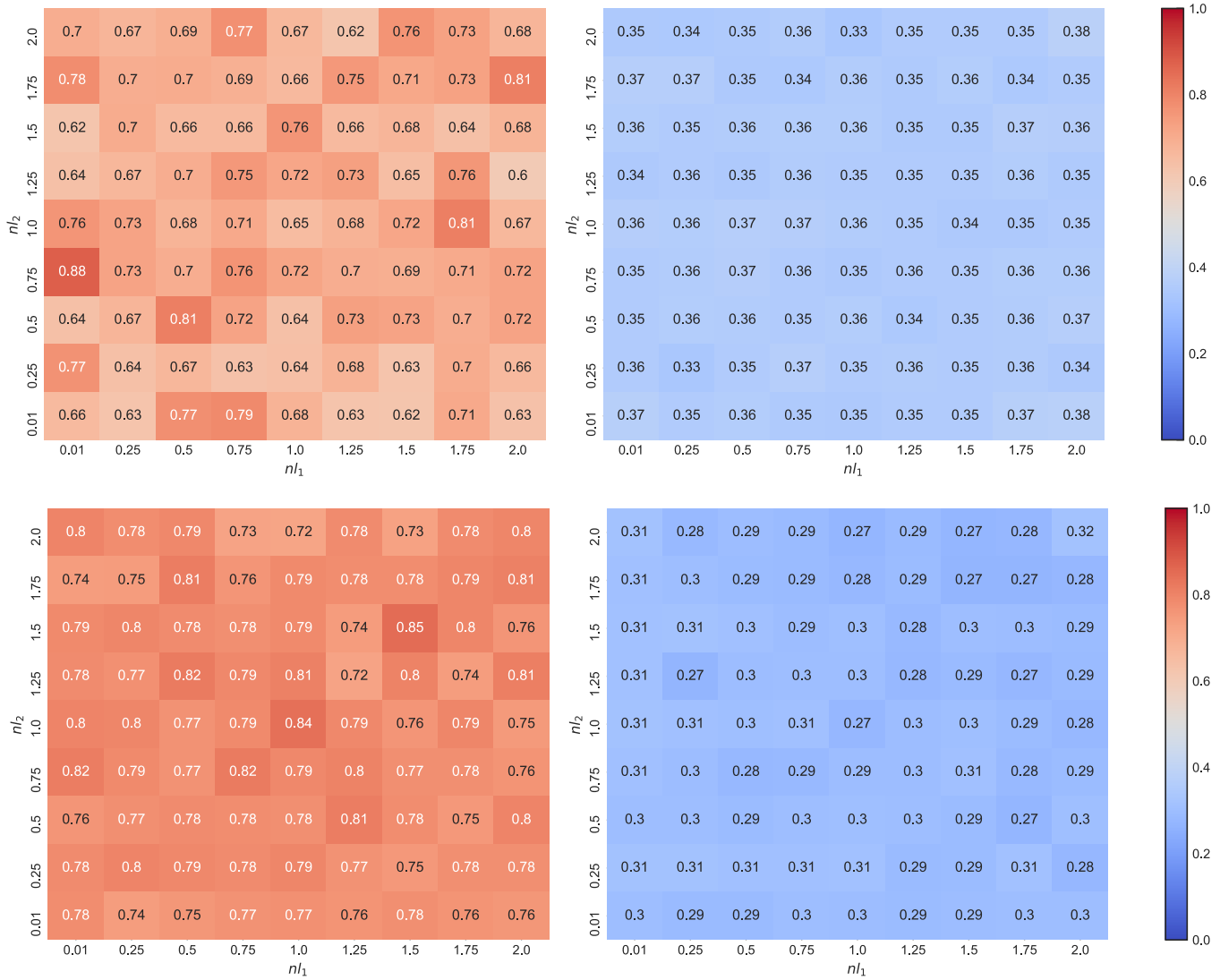

FIG. 7. TE (top row) and CCM (bottom row) causality of the Lorenz attractor for different degrees of nonlinearity. We compute the causalities for variations of λ_1 and λ_2 between 0.01 and 2, respectively. The left grids illustrate the original-causality while the right grid shows the surrogate-causality. All grid entries are averaged over 50 simulations under the standard configuration. The surrogate-causalities are averaged over $K = 10$ surrogate realizations.

Then, we merge the linear and nonlinear parts of the derivatives to construct the full governing equations,

$$\left(\frac{dx_j}{dt}\right) = \left(\frac{dx_j}{dt}\right)_{lin} + \left(\frac{dx_j}{dt}\right)_{nl}. \tag{23}$$

Finally, we assign coefficients to the individual terms and calibrate them to the data by using the gradient-descent based algorithm developed by Mariño and Míguez.[33]

IV. RESULTS

In the following, we present the results of our analysis, which are divided into four categories: Evaluation of causality matrices, nonlinear strength variation, analysis of causal structures, and derivation of governing equations.

A. Evaluation of causality matrices

Our analysis of the Lorenz and Halvorsen systems indicates that the causality is predominantly driven by nonlinear properties. This is illustrated in Fig. 5, where the box plots show that all surrogate-based causalities measured by TE and CCM are significantly lower than the original causality. This is because the surrogate time series only exhibit the same linear properties as the original time series while nonlinear effects are destroyed. We observe that a significant portion of TE and CCM can be attributed to nonlinear properties. As expected, we confirm that GC is indeed restricted to measuring linear causality as the original- and surrogate-GC are both on the same scale. The small deviations stem from the inaccuracies of the linear regression required for the calculation of GC. Analogously to Prichard and Theiler,[31] we repeat the calculation where we use different random phases when calculating the surrogate-GC between two time series. Since the surrogate-GC almost diminishes, we conclude that GC—just as Pearson correlation—only depends on phase differences. Furthermore, our developed anti- and cross-causalities, which measure the causal flow from the linear properties of one time series to both the linear and nonlinear properties of another, vanish for all three inference methods. This further suggests that the causal flows are mainly dominated by nonlinearity.

To verify that our method only measures linear and nonlinear causality when the governing equations are fully linear and nonlinear, we performed the analysis for the models given in Eqs. (3) and (4). Figure 6 highlights the validity of our methods, as the fully linear model has predominantly linear causality because GC is significant and the original and surrogate TE and CCM have similar strengths. For the fully nonlinear model, we observe the opposite case, where GC is low and the surrogate TE and CCM are significantly lower than the original TE and CCM.

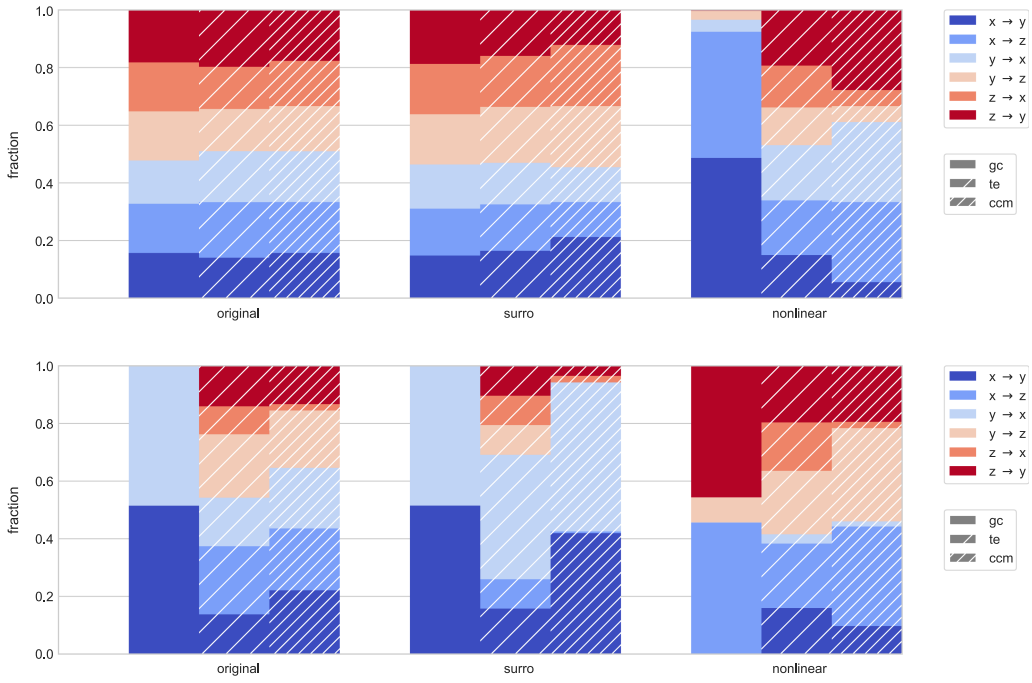

FIG. 8. Causality decomposition of the standard Lorenz (top row) and Halvorsen (bottom row) systems. For GC, TE, and CCM, we compute the original-, surrogate-, and nonlinear-causality, respectively. In order to obtain the contribution of each individual causal link to the causality of the whole system, we divide the causality of each link by the causality of the system. The contributions of the individual causal flows to the causality are mapped by color, while the different inference techniques are indicated by white stripes. The individual fractions are averaged over 50 simulations under the standard configuration. The surrogate-based causalities are averaged over $K = 10$ surrogate realizations.

B. Nonlinear strength variation

For the Lorenz and Halvorsen attractors, the analysis is repeated for variations in the degree of nonlinearity. While both systems diverge for nonlinearity degrees less or equal to 0, the upper bounds can be chosen arbitrarily as we do not observe significant changes to the attractor form. We conclude that the level of nonlinearity solely affects the scale of the attractors. Figure 2 illustrates the attractors for a selection of different parameter configurations. This behavior directly translates to the causality as indicated for the Lorenz system in Fig. 7. As expected, we find that the original causality is significantly larger than the surrogate causality for both TE and CCM across all degrees of nonlinearity. Furthermore, we observe that the grids show no visible gradient, which implies that the causality is independent of the degree of nonlinearity.

C. Analysis of causal structures

On a finer scale, we find that the causal structure of linear and nonlinear causality differs significantly for the Lorenz system, as illustrated in Fig. 9. We observe that the x and y pair is mainly driven by linear properties as it dominates the surrogate-causalities of GC and CCM—with both directions contributing equal amounts. In contrast, the surrogate-TE indicates that the direction x to y dominates the linear causality with a fraction of around 41%. This result is in line with the governing equations as the equation for x contains a linear contribution from y, while the equation for y contains a linear and nonlinear contribution from x. The rest of the system-causalities are more or less split evenly across the remaining flows.

In comparison, all flows in the Halvorsen attractor contribute approximately equally to the causality across all causality types and inference techniques, as depicted in Fig. 8. This causal structure is expected due to the circulant nature of the governing equations.

D. Derivation of governing equations

In order to verify our rationale, we apply it to the Lorenz and Halvorsen systems with their corresponding CCM-causal graphs, as computed from Eqs. (11) and (20), depicted in Fig. 9. The equations derived for the Lorenz system are

$$\begin{aligned} \frac{dx}{dt} &= y - x, \\ \frac{dy}{dt} &= x - xz - y, \\ \frac{dz}{dt} &= xy - z, \end{aligned} \tag{24}$$

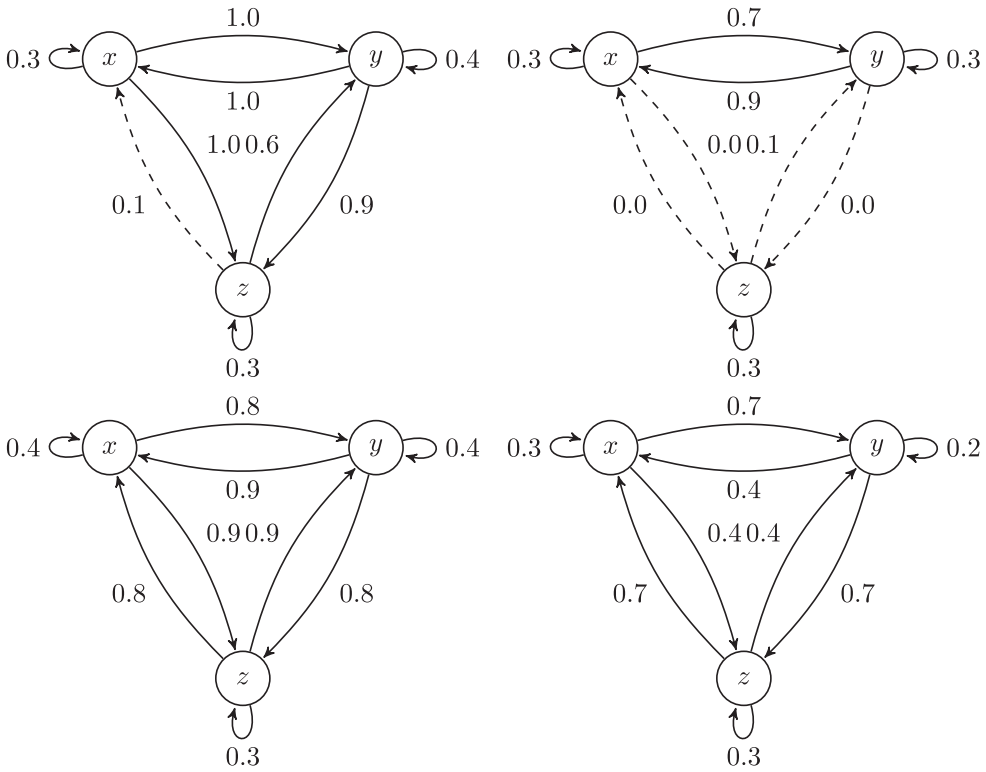

FIG. 9. CCM-causality graphs of the standard Lorenz (top row) and Halvorsen (bottom row) systems. The graphs depict the original (left) and the linear (right) CCM causality between the variables. The dashed lines indicate that the measured causality is not significant ($\theta < 0.1$). Note that the causalities in the loops are determined using the cross-CCM. The surrogate-based causal links on the right are averaged over $K = 10$ surrogate realizations.

TABLE I. Governing equations of the stock indices. This table depicts the derived governing equations for the six economies. The first column shows the time derivative of the economy while the second and third columns contain the linear and nonlinear terms before the COVID-19 outbreak, respectively. Analogously, the fourth and fifth columns contain the terms after the COVID-19 outbreak.

Economy	Before outbreak linear	Before outbreak nonlinear	After outbreak linear	After outbreak nonlinear
$\frac{dx_{eu}}{dt}$	$x_{eu} + x_{us} + x_{cn} + x_{ee} + x_{jp} + x_{px}$	$x_{eu}\ x_{px}$	$x_{eu} + x_{us} + x_{cn} + x_{ee} + x_{px}$	$x_{jp}x_{px} + x_{us}x_{cn} + x_{us}x_{ee} + x_{us}x_{jp} + x_{cn}x_{ee} + x_{cn}x_{jp} + x_{ee}x_{jp} + x_{ee}x_{px} + x_{ee}x_{px} + x_{cn}x_{px} + x_{us}x_{px}$
$\frac{dx_{us}}{dt}$	$x_{eu} + x_{us} + x_{cn} + x_{ee} + x_{jp} + x_{px}$	$x_{cn}\ x_{px}$	$x_{eu} + x_{us} + x_{cn} + x_{jp} + x_{px}$	$x_{cn}x_{px} + x_{ee}x_{px} + x_{cn}x_{ee}$
$\frac{dx_{cn}}{dt}$	$x_{eu} + x_{us} + x_{cn} + x_{ee} + x_{jp} + x_{px}$	$x_{eu}\ x_{us}$	$x_{cn} + x_{ee} + x_{px}$	$x_{eu}x_{ee} + x_{us}x_{ee} + x_{eu}x_{us} + x_{eu}x_{px} + x_{ee}x_{px} + x_{us}x_{px}$
$\frac{dx_{ee}}{dt}$	$x_{eu} + x_{us} + x_{cn} + x_{ee} + x_{jp} + x_{px}$	$x_{jp}\ x_{px}$	$x_{eu} + x_{us} + x_{cn} + x_{ee} + x_{jp} + x_{px}$	$x_{eu}x_{cn} + x_{us}x_{cn} + x_{jp}x_{px} + x_{us}x_{jp} + x_{cn}x_{jp} + x_{eu}x_{jp} + x_{eu}x_{us} + x_{eu}x_{px} + x_{cn}x_{px} + x_{us}x_{px}$
$\frac{dx_{jp}}{dt}$	$x_{cn} + x_{jp} + x_{px} + x_{eu}x_{ee}$	$x_{eu}x_{cn} + x_{us}x_{cn} + x_{us}x_{ee} + x_{cn}x_{jp} + x_{eu}x_{us} + x_{eu}x_{px} + x_{ee}x_{px} + x_{cn}x_{px} + x_{us}x_{jp}$	$x_{us} + x_{cn} + x_{ee} + x_{jp} + x_{px}$	$x_{us}x_{ee} + x_{eu}x_{us} + x_{eu}x_{ee}$
$\frac{dx_{px}}{dt}$	$x_{eu} + x_{cn} + x_{ee} + x_{jp} + x_{px}$	$x_{us}\ x_{px}$	$x_{eu} + x_{cn} + x_{ee} + x_{jp} + x_{px}$	$x_{us}x_{ee} + x_{eu}x_{us} + x_{eu}x_{ee}$

while the equations for the Halvorsen system are given by

$$\begin{aligned} \frac{dx}{dt} &= x - y - z - y^2, \\ \frac{dy}{dt} &= y - z - x - z^2, \\ \frac{dz}{dt} &= z - x - y - x^2. \end{aligned} \tag{25}$$

By comparing them to Eqs. (1) and (2), we find that our rationale reproduces the terms of the Lorenz and Halvorsen differential equations correctly. The calibration of the coefficients using the algorithm by Mariño and Míguez[33] yielded the correct coefficients $\sigma = 10$, $\rho = 28$, and $\beta = 8/3$ for the Lorenz system and $a = 1.3$ for the Halvorsen system with errors less than 1e−4, respectively.

These results are stable for thresholds $\theta < 0.2$. In order to ensure robustness, we repeat the analysis for different initial conditions and find that for a simulation length $T \geq 5000$ the causality inference and, hence, the equation derivation is stable.

In the following, we apply our rationale to a real-world system and derive the governing equations from the causal interactions between stock indices of six major economies: European Union, United States, China, Emerging Markets, Japan, and Pacific excluding Japan. The derived equations are shown in Table I, where we find that all economies except Japan have only one nonlinear term before the February 2020 COVID-19 pandemic outbreak. In contrast, the equations for the post-pandemic outbreak phase have at least three nonlinear terms in all economies, suggesting that nonlinearity has increased in the financial market. We find this result to be robust to changes in causal inference technique and thresholds $\theta < 0.2$. Furthermore, we would like to emphasize that we repeated the analysis, where we remap the rank-ordered time series onto a Gaussian distribution. Since the results remain practically unchanged, we conclude that our results are mainly driven by dynamic nonlinearities.

This result suggests that the COVID-19 pandemic has led to a fundamental change in the global financial market, which seems to make sense in light of the equity rally that was detached from the real economy.[34] Looking forward, as indicated by Haluszczynski *et al.*,[8] a large amount of nonlinearity in the market can potentially serve as an early indicator for financial crises.

Note that we do not assign coefficients to the individual terms of the equations as the calibration method by Mariño and Míguez[33] fails due to limited data and high dimensionality. Other equation derivation algorithms, such as Sparse Identification of Nonlinear Dynamics (SINDy),[12] also face this problem. SINDy is capable of generating equations with coefficients, but the equations diverge after a few simulation steps. Developing more sophisticated calibration methods to solve this problem is part of future research that is beyond the scope of this paper.

V. DISCUSSION

In this work, we analyzed the linear and nonlinear causal relations between variables in dynamical systems using different inference techniques and Fourier transform surrogates, which filter out the nonlinear properties of time series. We find for Lorenz and Halvorsen that nonlinearity is a key driver of causality and that nonlinear causality is independent of the strength of nonlinear terms in the governing equations. Furthermore, we developed a constructive and fully transparent rationale to derive the correct governing equations of the Lorenz and Halvorsen attractors directly from their causal structures—the resulting ease of interpretation is

the main advantage in comparison to black-box machine learning approaches. Finally, we applied our methods to stock indices from different economies and found that the outbreak of the COVID-19 pandemic triggered a structural change in the global financial markets.

This work can be extended in several directions. First, the provided framework can be deployed with further causal inference techniques and applied to other synthetic systems to confirm the universality of our results. Furthermore, new methods for calibrating the equation coefficients can be developed in order to address the problems of limited data and high dimensionality in real-world applications—this would enable precise predictions and the detection of unknown chaos and attractors.

ACKNOWLEDGMENTS

We would like to thank the DLR and Allianz Global Investors for providing data and computational resources.

AUTHOR DECLARATIONS

Conflict of Interest

The authors have no conflicts to disclose.

Author Contributions

Haochun Ma: Conceptualization (equal); Formal analysis (equal); Funding acquisition (equal); Methodology (equal); Software (equal); Visualization (equal); Writing – original draft (equal); Writing – review & editing (equal). **Alexander Haluszczynski:** Formal analysis (equal); Investigation (equal); Methodology (equal); Software (equal); Writing – review & editing (equal). **Davide Prosperino:** Formal analysis (equal); Software (equal); Visualization (equal); Writing – review & editing (equal). **Christoph Räth:** Conceptualization (equal); Methodology (equal); Supervision (equal); Writing – review & editing (equal).

DATA AVAILABILITY

The data that support the findings of this study are available from the corresponding author upon reasonable request.

REFERENCES

[1]H. R. Brown and D. Lehmkuhl, "Einstein, the reality of space and the action–reaction principle," in *Einstein, Tagore and the Nature of Reality* (Routledge, 2016), pp. 27–54.
[2]E. Lorenz, "The butterfly effect," in *World Scientific Series on Nonlinear Science Series A* (World Scientific, 2000), Vol. 39, pp. 91–94.
[3]C. W. Granger, *Essays in Econometrics: Collected Papers of Clive W.J. Granger* (Cambridge University Press, 2001), Vol. 32.
[4]T. Schreiber, "Measuring information transfer," Phys. Rev. Lett. **85**, 461 (2000).
[5]G. Sugihara, R. May, H. Ye, C.-h. Hsieh, E. Deyle, M. Fogarty, and S. Munch, "Detecting causality in complex ecosystems," Science **338**, 496–500 (2012).
[6]J. Runge, "Causal network reconstruction from time series: From theoretical assumptions to practical estimation," Chaos **28**, 075310 (2018).
[7]M. Paluš, V. Albrecht, and I. Dvořák, "Information theoretic test for nonlinearity in time series," Phys. Lett. A **175**, 203–209 (1993).
[8]A. Haluszczynski, I. Laut, H. Modest, and C. Räth, "Linear and nonlinear market correlations: Characterizing financial crises and portfolio optimization," Phys. Rev. E **96**, 062315 (2017).
[9]J. Hlinka, D. Hartman, M. Vejmelka, D. Novotná, and M. Paluš, "Non-linear dependence and teleconnections in climate data: Sources, relevance, nonstationarity," Clim. Dyn. **42**, 1873–1886 (2014).
[10]J. L. Breeden and A. Hübler, "Reconstructing equations of motion from experimental data with unobserved variables," Phys. Rev. A **42**, 5817 (1990).
[11]T. Eisenhammer, A. Hübler, N. Packard, and J. S. Kelso, "Modeling experimental time series with ordinary differential equations," Biol. Cybernet. **65**, 107–112 (1991).
[12]S. L. Brunton, J. L. Proctor, and J. N. Kutz, "Discovering governing equations from data by sparse identification of nonlinear dynamical systems," Proc. Natl. Acad. Sci. U.S.A. **113**, 3932–3937 (2016).
[13]B. C. Daniels and I. Nemenman, "Automated adaptive inference of phenomenological dynamical models," Nat. Commun. **6**, 1–8 (2015).
[14]K. Champion, B. Lusch, J. N. Kutz, and S. L. Brunton, "Data-driven discovery of coordinates and governing equations," Proc. Natl. Acad. Sci. U.S.A. **116**, 22445–22451 (2019).
[15]E. Hairer, S. P. Nørsett, and G. Wanner, *Solving Ordinary Differential Equations I* (Springer, 1993).
[16]E. N. Lorenz, "Deterministic nonperiodic flow," J. Atmos. Sci. **20**, 130–141 (1963).
[17]S. Vaidyanathan and A. T. Azar, "Adaptive control and synchronization of Halvorsen circulant chaotic systems," in *Advances in Chaos Theory and Intelligent Control* (Springer, 2016), pp. 225–247.
[18]V. P. Thoai, M. S. Kahkeshi, V. V. Huynh, A. Ouannas, and V.-T. Pham, "A nonlinear five-term system: Symmetry, chaos, and prediction," Symmetry **12**, 865 (2020).
[19]S. L. Bressler and A. K. Seth, "Wiener–Granger causality: A well established methodology," Neuroimage **58**, 323–329 (2011).
[20]L. Barnett, A. B. Barrett, and A. K. Seth, "Granger causality and transfer entropy are equivalent for Gaussian variables," Phys. Rev. Lett. **103**, 238701 (2009).
[21]M. Mynter, "Evaluation and extension of the transfer entropy calculus for the measurement of information flows between futures time series during the COVID-19 pandemic," Master thesis (Ludwig-Maximilians-Universität München, 2021) (unpublished).
[22]S. Baur and C. Räth, "Predicting high-dimensional heterogeneous time series employing generalized local states," Phys. Rev. Res. **3**, 023215 (2021).
[23]M. Paluš and M. Vejmelka, "Directionality of coupling from bivariate time series: How to avoid false causalities and missed connections," Phys. Rev. E **75**, 056211 (2007).
[24]J. M. McCracken and R. S. Weigel, "Convergent cross-mapping and pairwise asymmetric inference," Phys. Rev. E **90**, 062903 (2014).
[25]M. B. Kennel, R. Brown, and H. D. Abarbanel, "Determining embedding dimension for phase-space reconstruction using a geometrical construction," Phys. Rev. A **45**, 3403 (1992).
[26]B. Cummins, T. Gedeon, and K. Spendlove, "On the efficacy of state space reconstruction methods in determining causality," SIAM J. Appl. Dyn. Syst. **14**, 335–381 (2015).
[27]L. Overbey and M. Todd, "Effects of noise on transfer entropy estimation for damage detection," Mech. Syst. Signal Process. **23**, 2178–2191 (2009).
[28]P. Krishna and A. K. Tangirala, "Inferring direct causality from noisy data using convergent cross mapping," in *2019 58th Annual Conference of the Society of Instrument and Control Engineers of Japan (SICE)* (IEEE, 2019), pp. 1523–1528.
[29]C. Räth and R. Monetti, "Surrogates with random Fourier phases," in *Topics on Chaotic Systems: Selected Papers from Chaos 2008 International Conference* (World Scientific, 2009), pp. 274–285.
[30]C. Räth, M. Gliozzi, I. Papadakis, and W. Brinkmann, "Revisiting algorithms for generating surrogate time series," Phys. Rev. Lett. **109**, 144101 (2012).
[31]D. Prichard and J. Theiler, "Generating surrogate data for time series with several simultaneously measured variables," Phys. Rev. Lett. **73**, 951 (1994).
[32]X. Wan, W. Wang, J. Liu, and T. Tong, "Estimating the sample mean and standard deviation from the sample size, median, range and/or interquartile range," BMC Med. Res. Methodol. **14**, 1–13 (2014).
[33]I. P. Mariño and J. Míguez, "An approximate gradient-descent method for joint parameter estimation and synchronization of coupled chaotic systems," Phys. Lett. A **351**, 262–267 (2006).
[34]J. Cox, D. L. Greenwald, and S. C. Ludvigson, "What explains the COVID-19 stock market?" Technical Report, National Bureau of Economic Research, 2020.